3D electron diffraction reveals the chiral nature of the malaria pigment crystal hemozoin

Paul Benjamin Klar[1*], David Waterman[2*], Tim Gruene[3*], Debakshi Mullick[4], Yun Song[5], James B. Gilchrist[5], Wen Wen[6], Idan Biran[7], Lothar Houben[8], Neta Regev-Rudzki[9], Ron Dzikowski[10], Noa Marom[11], Lukas Palatinus[1], Peijun Zhang[5,12], Leslie Leiserowitz[7], Michael Elbaum[4]

[1]Institute of Physics of the Czech Academy of Sciences, Na Slovance 2
182 21 Prague 8, Czechia

[2]STFC, Rutherford Appleton Laboratory, Didcot OX11 0FA, UK, and
CCP4, Research Complex at Harwell, Rutherford Appleton Laboratory, Didcot OX11 0FA, UK

[3]Department of Inorganic Chemistry, Faculty of Chemistry, University of Vienna
Vienna, Austria

[4]Department of Chemical and Biological Physics, Weizmann Institute of Science
76100 Rehovot, Israel

[5]Diamond Light Source, Harwell Science and Innovation Campus,
Didcot OX11 0DE, UK

[6]Department of Chemistry, Carnegie Mellon University
Pittsburgh, Pennsylvania 15213 USA

[7]Department of Molecular Chemistry and Materials Science, Weizmann Institute of Science
76100 Rehovot, Israel

[8]Department of Chemical Research Support, Weizmann Institute of Science
76100 Rehovot, Israel

[9]Department of Biomolecular Sciences, Weizmann Institute of Science
76100 Rehovot, Israel

[10]Department of Microbiology and Molecular Genetics, Institute for Medical Research Israel-Canada, and The Kuvin Center for the Study of Infectious and Tropical Diseases, The Hebrew University-Hadassah Medical School
Jerusalem, Israel

[11]Department of Materials Science and Engineering, Carnegie Mellon University
Pittsburgh, Pennsylvania 15213 USA

[12]Division of Structural Biology, Wellcome Trust Centre for Human Genetics, University of Oxford, Oxford, OX3 7BN, UK

[*]equal contribution

Paul Benjamin Klar present address: University of Bremen, Faculty of Geosciences,
Klagenfurter Str. 2-4, 28359 Bremen, Germany

Abstract

Detoxification of heme in Plasmodium and other blood-borne parasites results in crystallization of hemozoin. This crystallization is a major target of antimalarial drugs. The structure of hemozoin has been studied primarily by X-ray powder diffraction, which showed that the unit cell contains a centrosymmetric cyclic hematin dimer. The pro-chiral nature of heme would support formation of two centrosymmetric and two enantiomeric chiral dimer structures. Here we apply emerging methods of cryo-electron microscopy, tomography, and diffraction to obtain a definitive structure of biogenic hemozoin. Individual crystals typically take a polar shape with morphology distinct from that of the more commonly-studied synthetic form. Diffraction analysis and density functional theory indicate a compositional mixture of one centrosymmetric and one chiral dimer, whose absolute configuration has been determined on the basis of crystal morphology and interaction with the aqueous medium. Structural modeling of the heme detoxification protein suggests a mechanism for such enantiomeric selection in dimer production. The refined structure of native hemozoin should serve as a guide to new drug development.

Malaria is a deadly disease that remains endemic to much of the world despite extraordinary efforts to its eradication (World Health Organization, 2021). Anopheles mosquitos are the common vector, and several species of Plasmodium affect humans, where they infect the red blood cells. While the parasite catabolizes the hemoglobin protein as a source of biomolecules, it has no mechanism to degrade the toxic heme released in the process. In common with a number of other blood-borne parasites, Plasmodium detoxifies the heme by sequestration into physiologically insoluble crystals of hemozoin, also known diagnostically as the malaria pigment. Disease symptoms include anemia and severe paroxysms resulting from immune response to hemozoin released to the blood stream (Olivier et al., 2014). Nucleation and growth of hemozoin in the parasite is a target of common antimalarial drugs. Therefore, a precise determination of the crystal structure and morphology is of prime medical importance as well as fundamental interest.

A landmark study by X-ray powder diffraction (XRPD) revealed the crystalline structure of synthetic hemozoin, known as β-hematin (Pagola et al., 2000). The unit cell contains not the monomeric heme present in hemoglobin, but rather a cyclic dimer. The structure was refined in a triclinic $P\bar{1}$ arrangement with one dimer per unit cell. Cyclic H-bonds between propionic acid groups form chains linking the hematin dimers along the ***a***–***c*** direction. The growth morphology is rod-like with well-developed {100} faces and {010} side faces of variable width. Crystal ends are capped by slanted {011} faces, as determined by transmission electron microscopy and diffraction (Solomonov et al., 2007). Morphology of the synthetic crystal is in agreement with a theoretical growth form based on attachment energies (Buller et al., 2002).

While the model structure of β-hematin was centrosymmetric, the pro-chiral nature of the heme supports four configurations of the dimer (Buller et al., 2002; Marom et al., 2010; Straasø et al., 2014, 2011). Specifically, methyl – vinyl pairs opposite the propionic acids are arranged asymmetrically, defining *re* (*rectus*) and *si* (*sinister*) heme faces. Heme binding proteins typically distinguish these two inequivalent orientations (Schneider et al., 2007). Cyclic dimers form distinct isomers depending on which heme faces are brought to contact: *R*/*S*′, *S*/*R*′, *R*/*R*′, or *S*/*S*′. The first two are centrosymmetric, whereas the latter two are chiral enantiomers with pseudo-centrosymmetry (Fig. 1, Fig. S3). Straasø et al. interpreted XRPD data of synthetic hemozoin in terms of a major and minor centrosymmetric phase and suggested that these represent *R*/*S*′ and *S*/*R*′ isoforms, each containing additionally *R*/*R*′ and *S*/*S*′ dimers (Straasø et al., 2014). Bohle et al. then reanalyzed the earlier powder diffraction and interpreted the data in terms of a disordered structure of *R*/*S*′ and *S*/*R*′ dimers in a 3:1 ratio (Bohle et al., 2012). Complementary evidence that synthetic hemozoin is comprised of a mixture of the different isomeric hematin dimers also stemmed from a single-crystal X-ray diffraction study of a hematin dimer-DMSO solvate (Gildenhuys et al., 2013). More recently, a study of synthetic hemozoin by X-ray free electron laser diffraction (Dilanian et al., 2017) suggested that the structure of nano-crystals may differ from that of larger crystals due to greater conformational flexibility in the propionic chains. This might also be interpreted as a difference in isomeric composition (Kapishnikov et al., 2021).

For the case of biogenic hemozoin, a chiral model of the hematin dimer was proposed by Straasø et al. (2014) on the assumption that the heme, upon release from oxygenated hemoglobin, retained the O_2 molecule enantiotopically coordinated to the Fe(II) ion. An XRPD analysis of the crystal structure modeled as a mixture of chiral (*S*/*S*′) and centrosymmetric (*R*/*S*′) dimers, was, however, insufficiently conclusive.

Whole cell cryo-tomography using soft X-rays revealed biogenic hemozoin in the parasite digestive vacuole (Kapishnikov et al., 2012b), and focused X-ray diffraction could suggest a preferential growth orientation (Kapishnikov et al., 2012a). Recently developed cryogenic scanning transmission electron tomography (CSTET) provides a higher resolution view (Elbaum et al., 2021; Mullick et al., 2022; Wolf et al., 2014), while the development of 3D electron diffraction (3D ED) with narrow-field illumination makes it feasible to record diffraction patterns from sub-micron size specimens (Beale et al., 2020; Gemmi et al., 2019; Gruene et al., 2018; Jones et al., 2018). In this work we enlist the new methods to address the crystal structure of biogenic hemozoin.

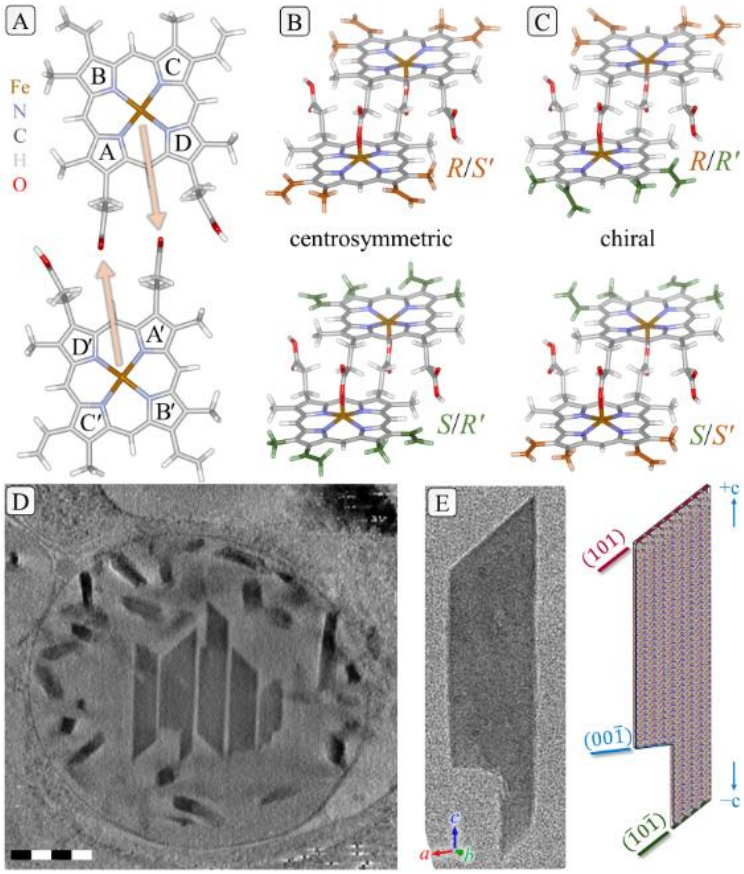

Figure 1. (A). Prior to crystallization, two heme monomers interlink to form cyclic hematin dimers via the binding of each central Fe ion to one of the two propionic acid tails (pyrrole ring labels included). The pro-chiral nature of the heme supports formation of four isomers. (B). Centrosymmetric *R*/*S*′ and *S*/*R*′ dimers differ in binding of the Fe to the propionate $CH_2CH_2C(=O)O$- moiety at the A or D pyrrole. (C). *R*/*R*′ and *S*/*S*′ are enantiomers. Colors of methyl and vinyl groups indicate the symmetrical relationship: both sides either orange or green for centrosymmetry and mixed for chiral dimers. See also Supplementary Fig. S3. (D). Thick virtual section from a tomographic reconstruction of an intact digestive vacuole showing large crystals in the center and numerous smaller crystals decorating the periphery. Note the polar shapes of the crystals. The complete reconstruction appears in Supplementary Movie S1. Scale bar 500 nm. (E). An exemplary crystal used in the diffraction study, with annotation of faces by *hkl* indices.

Infected red blood cells were deposited and burst directly on electron microscope grids, and then immediately vitrified. CSTET reconstructions of intact parasites revealed that opposite ends of hemozoin typically differ: one end shows a smooth chisel shape while the other is variable, usually squared off or ragged with an overhang (Fig. 1D). Similar shapes have been observed previously, either without comment (Ambele et al., 2013; Noland et al., 2003) or with suggestion that the ragged end represents the site of growth (Wendt et al., 2021). A purely centrosymmetric crystal structure should not produce such a polar morphology. Where individual crystals were dispersed from ruptured cells, conventional TEM images were recorded of narrow fields of view and diffraction data collected at −178 °C in continuous tilt mode over a range of 90°. Indexing the crystal faces yielded the surprising result that the end cap orientations are not $\{011\}$, as seen in synthetic hemozoin, but rather (101) and $(00\bar{1})$, or (101) and a combination of $(\bar{1}0\bar{1})$, $(00\bar{1})$, and nearby low index directions (Fig. 1E, Fig. S1). Details appear in Supplementary Section 2.

A complete set of 3992 Friedel-related hkl and $\bar{h}\bar{k}\bar{l}$ reflections was obtained from 36 individual crystals (Fig. S2). The scaled intensities of corresponding reflections matched very well despite differences in crystal size, indicating the presence of only a single crystalline phase for biogenic hemozoin. Lattice parameters of biogenic hemozoin at low temperature were adopted from Straasø et al (Straasø et al., 2014). Preliminary analysis was performed using DIALS (Clabbers et al., 2018; Winter et al., 2018) and model structures of all four hematin dimers were each refined by least-squares electron structure factor analysis (Supplementary Section 3) (Sheldrick, 2015). The refinement cannot distinguish the chiral enantiomers, whereas the centrosymmetric dimers differ in the coordination of the propionic acid on the *A* or *D* pyrrole to the neighboring Fe. Given the polar crystal habits, the *R*/*S*′ and *S*/*R*′ dimers were not constrained as centrosymmetric entities. Overall *R* factor and atomic displacement parameters appear in Table S3. The fit of the *S*/*R*′ model was considerably worse than the others. The crystal structure embodying the chiral dimer refined with fewest inconsistencies. All parameters refined well except the displacement parameters of terminal carbons in the vinyl substituents on the B′ and C′ pyrrole groups belonging specifically to the lower primed hematin ring, as depicted in Fig. 2B. The related carbons on the upper monomer appeared sharp, however. A simple explanation is that the crystal structure contains a mixture of dimers, one chiral and one centrosymmetric. This would account for the perfect atomic overlay on one side and the loss of atomic localization on the other for both the *R*/*R*′ and the *R*/*S*′ dimer. For roughly equal dimer occupancy, displacement parameters for the vinyl substituents were consistent with those of other constituent atoms. Additionally, all the vinyl groups assumed the more prevalent *cis* conformation, except for one that took a *trans* orientation. A further refinement based on dynamical diffraction analysis (Supplementary Section 4) confirmed the disordered model as well as 1:1 occupancy of *R*/*S*′ and chiral dimers, shown in Fig. 2C,D.

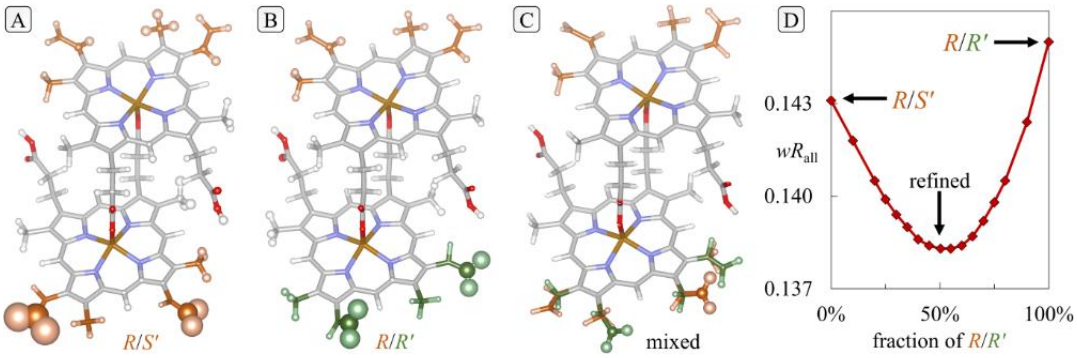

Figure 2. Refinement of the different dimers reveals a mix of chiral and centrosymmetric dimers. Atom spheres and ellipsoids represent displacement probability surfaces at the 10% level. (A). The centrosymmetric *R*/*S*′ model refines well except for the vinyl groups of a single monomer. (B). The chiral *R*/*R*′ model shows smaller displacement parameters, and a single vinyl in the *trans* conformation. (C). All atoms refine well in a structure containing a mixture of *R*/*R*′ and *R*/*S*′ dimers. (D). R-factors of dynamical refinements with fixed composition indicate an equal concentration of *R*/*S'* and *R*/*R'* dimers in the structure.

Density functional theory (DFT) calculations with the many-body dispersion (MBD) method (Tkatchenko et al., 2012) were performed to confirm: a) the plausibility of an isomerically mixed crystal, and b) the *trans* orientation of one vinyl group belonging to a chiral dimer. Full unit cell relaxation was performed for crystals comprising pure and mixed dimers. Results are summarized in Fig. 3; details appear in Supplementary Section 5. The outcome of DFT+MBD analysis, that the biogenic hemozoin crystal can easily comprise a mixture of *R*/*S*′ and one chiral dimer, supports the experimentally derived results. Other combinations have higher energy and are therefore less likely to occur. For the chiral dimer specifically, the vinyl on the C pyrrole is indeed in a *trans* conformation and the other three vinyl groups take a *cis* conformation. We attribute this to intermolecular forces in the crystal, which stabilize the otherwise less stable *trans* conformation.

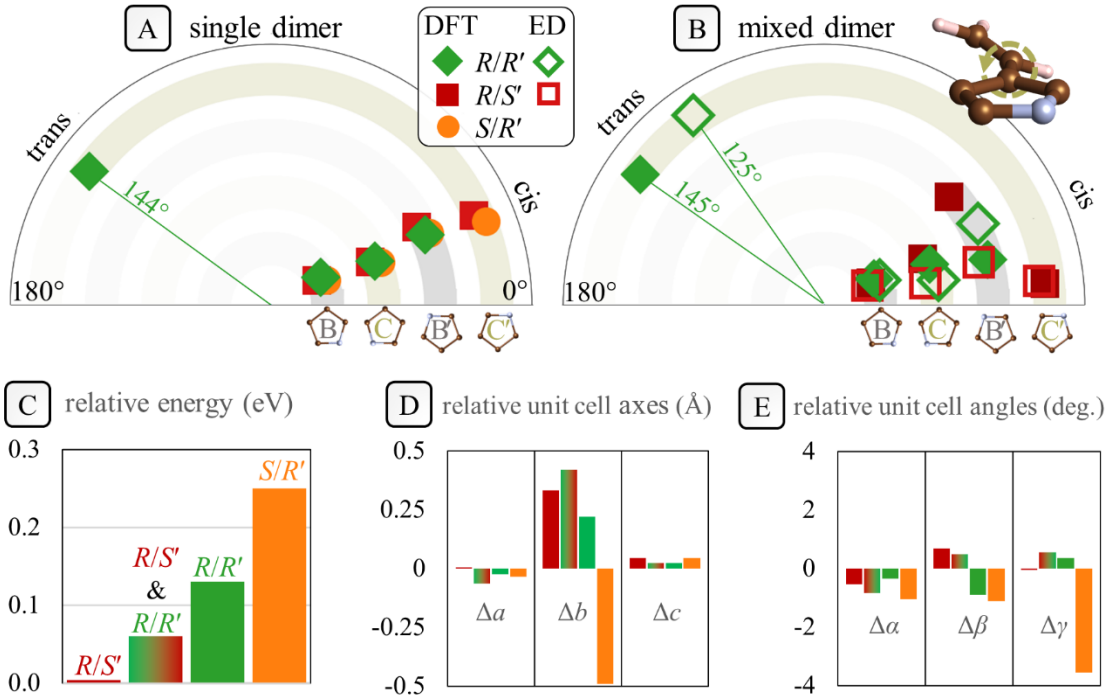

Figure 3. Results of DFT calculations. (A) All vinyl groups take the *cis* configuration, except for a single *trans* vinyl on the C′ pyrrole of the *R*/*R*′ dimer (see Fig. 1). (B) In the mixed *R*/*S*′+*R*/*R*′ crystal, again DFT predicts a single *trans* vinyl on the *R*/*R*′ dimer, in agreement with experiment (ED). (C) Energy rankings of the various models tested. (D) Unit cell parameters of the optimised structures in comparison with measurement (Straasø et al., 2014). Color labels as in (C). Note the poor fit of the *S*/*R*′ dimer.

In principle, the interference of simultaneously excited beams within the crystal makes the diffracted intensities sensitive to the absolute structure (Klar et al., 2021). The effect is weak, however, given that mainly the terminal, half occupied vinyl CH_2 groups contribute to the chirality, and we have been unable to discriminate the handedness with presently available methods (Tab. S5).

We may nonetheless deduce the absolute structure on the basis of morphology (Weissbuch et al., 1983). A crystal composed purely of centrosymmetric *R*/*S*′ dimers should adopt a nonpolar habit, yet we observe a pronounced variability at one end. As seen in Fig. 1, the habit is polar, with a (101) face at the +*c* end and often a short $(00\bar{1})$ face at the −*c* end; other crystals show a mixed shape at −*c* with a ragged $(00\bar{1})$ facet and a decidedly longer handle-shaped segment capped by a $(\bar{1}0\bar{1})$ facet (Figs. 1D and S1). Considering that the carboxyl pairs form H-bonded acid chains which run parallel to (101) and $(\bar{1}0\bar{1})$, water in the aqueous medium of the digestive vacuole will bind poorly to either face. By comparison, the carboxyl and carboxylate groups at the $(00\bar{1})$ face are well exposed (Figs. 4 and S4-S6), so that growth of this face will be inhibited by competitive binding of water molecules. This explains why the habit of biogenic crystals differs from that of synthetic hemozoin grown in organic solvent (capped by $\{011\}$ faces), and also why the $(\bar{1}0\bar{1})$ facet grows faster than $(00\bar{1})$. Considering the mixed crystal to be composed of *R*/*S*′ + *R*/*R*′ hematin dimers, atomic disorder will occur at the +b face and the −*c* end of the rod. Local inhomogeneities in composition could then explain the variable

formation of the $(\bar{1}0\bar{1})$ and $(00\bar{1})$ facets, reflecting centrosymmetric or polar structure (Fig. S1).

Morphological analysis of biogenic hemozoin recalls the assignment of molecular chirality in centrosymmetric crystals composed of a mixture of chiral *R* and *S* molecules grown in the presence of a tailor-made chiral inhibitor (*R*′ or *S*′) (Weissbuch et al., 1983). In this regard, we present here the first reported case of such assignment of handedness for a molecule of unknown chirality.

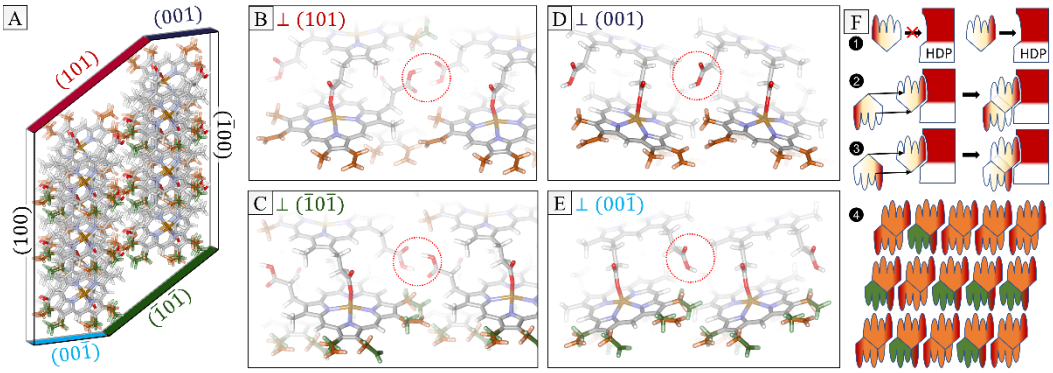

Figure 4. Groups exposed at the surfaces of hemozoin crystals composed of a mixture of *R*/*S*′ + *R*/*R*′ dimers. (A). Array of unit cells as visual guide. The mixture appears as disorder on the $(00\bar{1})$ and $(\bar{1}0\bar{1})$ surfaces, but the (001) and (101) surfaces are completely ordered. (B-E). A detailed view of the methyl-vinyl pairs on the various exposed surfaces. Additionally, the carboxyl and carboxylate groups are exposed to the aqueous medium at the $(00\bar{1})$ surface, rendering it more hydrophilic than the (101) and $(\bar{1}0\bar{1})$ surfaces where the available bonds are saturated and buried (red circles, fading represents depth). Crystal growth of the relatively hydrophilic $(00\bar{1})$ face will be inhibited by competitive binding of water. (F). A model for the function of HDP. A chiral agent that binds preferentially to one monomer orientation generates one chiral and one centrosymmetric dimer, resulting in a polar crystal where disorder appears on one or the other side, but not on both.

In another approach, we performed through-focus imaging and phase retrieval on a crystal in a favorable orientation viewing along the −***a*** direction where the vinyl-methyl groups are visible in otherwise empty channels. Multi-slice simulations using the refined models generated in the dynamical diffraction analysis yielded a superior fit to the data for the mixture containing the *R*/*R*′ rather than the *S*/*S*′ chiral dimer (Supplementary Section 6).

The selection of one chiral and one centrosymmetric dimer implies the presence of a chiral agent in their formation. The heme detoxification protein (HDP) is associated with falcipain 2 and other proteases, and has been implicated as a catalyst for dimerization between steps of hemoglobin digestion and hemozoin crystallization (Chugh et al., 2013). Biochemical studies indicated the presence of at least two binding sites involving four key histidine residues: His122 and His197 form one site, while His172 and His175 form another, with Fe binding only His122 (Nakatani et al., 2014, 2013). To date there is no high-resolution molecular structure available for HDP, although it is recognized to have a fascilin-like fold. Therefore, we turned to structural modeling (Supplementary Section 7). There was a broad consensus at high confidence in the

architectural features, with a compact α-helical domain at the N terminus and a largely unfolded cap at the C terminus (Fig. S9). One heme binding site containing the Fe-binding histidine appears in a pocket between the compact core of the protein and the cap, while the other appears at the tip of a long unfolded loop. The dimerization reaction will occur between these two His-bound hemes. If chiral discrimination at the protein core fixes the orientation of one heme, then topologically, only one chiral dimer may form (Fig. 3F, Fig. S10).

An earlier model proposed the formation of a chiral *S*/*S*' dimer if heme remains oxygenated after liberation from hemoglobin (Straasø et al., 2014). Binding of oxygenated heme to HDP via His122 would reverse the orientation, resulting in the *R*/*R*' dimer (See Fig. S9 in (Kapishnikov et al., 2021)). Diffraction data reported here were obtained from crystals in cells grown at low atmospheric oxygen (1%), corresponding to oxygen saturation of hemoglobin below 10%. While oxygenation could not have played a substantial role in obtaining the 50:50 mixture, the trends for oxygenation and putative chiral recognition in HDP operate in tandem to favor the formation of an *R*/*R*' dimer.

In summary, tomography, diffraction, density functional theory, morphological analysis and through-focus imaging combine to yield a refined structure of native hemozoin from Plasmodium falciparum. The crystal structure contains a mixture of hematin dimers, one centrosymmetric and one chiral, and previously unrecognized, deeply corrugated (101) and $(\bar{1}0\bar{1})$ surfaces. This definitive structure should serve as a template for development of treatments for malaria where hemozoin is a drug target.

Author contributions

DM prepared samples provided by RD and NRR. DM, JG, and YS acquired and analyzed data under supervision of PZ. DW and TG analysed diffraction data within the kinematical approximation. PK and LP refined the structure by dynamical diffraction methods. WW and NM performed DFT calculations. IB and LH contributed the phase retrieval from real space imaging. ME and LL coordinated the project and wrote the paper, with extensive cooperation of the authors.

Acknowledgements

We thank Jens Als Nielsen for a critical reading of the manuscript and Isabella Weissbuch for inspiring discussions. This work was funded in part by grants to ME from the Minerva Foundation, the Israel Science Foundation (project 1696/18), and the Estate of David Levinson, to LP from the Czech Science Foundation (project 21-05926X) and the Czech Ministry of Education, Youth and Sports, LM2018110 (CzechNanoLab Research Infrastructure). ME is Head of the Irving and Cherna Moskowitz Center for Nano and Bionano Imaging and incumbent of the Sam and Ayala Zacks Professorial Chair in Chemistry. We acknowledge Diamond for access and support of the cryoEM facilities at the U.K. national electron Bio-Imaging Centre (eBIC) (proposals NT21004 and NT29812), funded by the Wellcome Trust, MRC, and BBSRC. Work at CMU was supported by the National Science Foundation (NSF) Division of Materials Research (DMR) through grant DMR-2131944. This research used computational resources of the National Energy Research Scientific Computing Center (NERSC), a DOE Office of Science User Facility supported by the Office of Science of the U.S. Department of Energy, under Contract DE-AC02-05CH11231; the Argonne Leadership Computing Facility (ALCF), which is a DOE Office of Science User Facility supported under Contract DE-AC02-06CH11357; and the Extreme Science and Engineering Discovery Environment (XSEDE), which is supported by National Science Foundation grant number ACI-1548562. This work was supported in part by the Wellcome Trust Investigator Award (206422/Z/17/Z) and the ERC AdG grant (101021133).

For the purpose of open access, the authors have applied a Creative Commons Attribution (CC BY) licence to any Author Accepted Manuscript version arising.

All data needed to evaluate the conclusions in the paper are present in the paper and/or the Supplementary Materials. Diffraction datasets are published at https://doi.org/10.5281/zenodo.5039355.

Bibliography

Ambele, M.A., Sewell, B.T., Cummings, F.R., Smith, P.J., Egan, T.J., 2013. Synthetic Hemozoin (β-Hematin) Crystals Nucleate at the Surface of Neutral Lipid Droplets that Control Their Sizes. Crystal Growth & Design 13, 4442–4452. https://doi.org/10.1021/cg4009416

Beale, E.V., Waterman, D.G., Hecksel, C., van Rooyen, J., Gilchrist, J.B., Parkhurst, J.M., de Haas, F., Buijsse, B., Evans, G., Zhang, P., 2020. A Workflow for Protein Structure Determination From Thin Crystal Lamella by Micro-Electron Diffraction. Frontiers in Molecular Biosciences 7, 179. https://doi.org/10.3389/fmolb.2020.00179

Bohle, D.S., Dodd, E.L., Stephens, P.W., 2012. Structure of Malaria Pigment and Related Propanoate-Linked Metalloporphyrin Dimers. Chemistry & Biodiversity 9, 1891–1902. https://doi.org/10.1002/cbdv.201200033

Buller, R., Peterson, M.L., Almarsson, Ö., Leiserowitz, L., 2002. Quinoline Binding Site on Malaria Pigment Crystal: A Rational Pathway for Antimalaria Drug Design. Crystal Growth & Design 2, 553–562. https://doi.org/10.1021/cg025550i

Chugh, M., Sundararaman, V., Kumar, S., Reddy, V.S., Siddiqui, W.A., Stuart, K.D., Malhotra, P., 2013. Protein complex directs hemoglobin-to-hemozoin formation in Plasmodium falciparum. Proc Natl Acad Sci U S A 110, 5392–5397. https://doi.org/10.1073/pnas.1218412110

Clabbers, M.T.B., Gruene, T., Parkhurst, J.M., Abrahams, J.P., Waterman, D.G., 2018. Electron diffraction data processing with DIALS. Acta Cryst D 74, 506–518. https://doi.org/10.1107/S2059798318007726

Dilanian, R.A., Streltsov, V., Coughlan, H.D., Quiney, H.M., Martin, A.V., Klonis, N., Dogovski, C., Boutet, S., Messerschmidt, M., Williams, G.J., Williams, S., Phillips, N.W., Nugent, K.A., Tilley, L., Abbey, B., 2017. Nanocrystallography measurements of early stage synthetic malaria pigment. J Appl Cryst 50, 1533–1540. https://doi.org/10.1107/S1600576717012663

Elbaum, M., Seifer, S., Houben, L., Wolf, S.G., Rez, P., 2021. Toward Compositional Contrast by Cryo-STEM. Acc. Chem. Res. https://doi.org/10.1021/acs.accounts.1c00279

Gemmi, M., Mugnaioli, E., Gorelik, T.E., Kolb, U., Palatinus, L., Boullay, P., Hovmöller, S., Abrahams, J.P., 2019. 3D Electron Diffraction: The Nanocrystallography Revolution. ACS Cent. Sci. 5, 1315–1329. https://doi.org/10.1021/acscentsci.9b00394

Gildenhuys, J., Roex, T. le, Egan, T.J., de Villiers, K.A., 2013. The Single Crystal X-ray Structure of β-Hematin DMSO Solvate Grown in the Presence of Chloroquine, a β-Hematin Growth-Rate Inhibitor. J. Am. Chem. Soc. 135, 1037–1047. https://doi.org/10.1021/ja308741e

Gruene, T., Wennmacher, J.T.C., Zaubitzer, C., Holstein, J.J., Heidler, J., Fecteau-Lefebvre, A., De Carlo, S., Müller, E., Goldie, K.N., Regeni, I., Li, T., Santiso-Quinones, G., Steinfeld, G., Handschin, S., van Genderen, E., van Bokhoven, J.A., Clever, G.H., Pantelic, R., 2018. Rapid Structure Determination of Microcrystalline Molecular Compounds Using Electron Diffraction. Angewandte Chemie International Edition 57, 16313–16317. https://doi.org/10.1002/anie.201811318

Jones, C.G., Martynowycz, M.W., Hattne, J., Fulton, T.J., Stoltz, B.M., Rodriguez, J.A., Nelson, H.M., Gonen, T., 2018. The CryoEM Method MicroED as a Powerful Tool for Small Molecule Structure Determination. ACS Cent. Sci. 4, 1587–1592. https://doi.org/10.1021/acscentsci.8b00760

Kapishnikov, S., Berthing, T., Hviid, L., Dierolf, M., Menzel, A., Pfeiffer, F., Als-Nielsen, J., Leiserowitz, L., 2012a. Aligned hemozoin crystals in curved clusters in malarial red blood cells revealed by nanoprobe X-ray Fe fluorescence and diffraction. PNAS 109, 11184–11187. https://doi.org/10.1073/pnas.1118134109

Kapishnikov, S., Hempelmann, E., Elbaum, M., Als-Nielsen, J., Leiserowitz, L., 2021. Malaria Pigment Crystals: The Achilles' Heel of the Malaria Parasite. ChemMedChem 16, 1515–1532. https://doi.org/10.1002/cmdc.202000895

Kapishnikov, S., Weiner, A., Shimoni, E., Guttmann, P., Schneider, G., Dahan-Pasternak, N., Dzikowski, R., Leiserowitz, L., Elbaum, M., 2012b. Oriented nucleation of hemozoin at the digestive vacuole membrane in Plasmodium falciparum. PNAS 109, 11188–11193. https://doi.org/10.1073/pnas.1118120109

Klar, P., Krysiak, Y., Xu, H., Steciuk, G., Cho, J., Zou, X., Palatinus, L., 2021. Chirality and accurate structure models by exploiting dynamical effects in continuous-rotation 3D ED data. ChemRxiv. https://doi.org/10.26434/chemrxiv-2021-4jh14

Marom, N., Tkatchenko, A., Scheffler, M., Kronik, L., 2010. Describing Both Dispersion Interactions and Electronic Structure Using Density Functional Theory: The Case of Metal-Phthalocyanine Dimers. J Chem Theory Comput 6, 81–90. https://doi.org/10.1021/ct900410j

Mullick, D., Rechav, K., Leiserowitz, L., Regev-Rudzki, N., Dzikowski, R., Elbaum, M., 2022. Diffraction contrast in cryo-scanning transmission electron tomography reveals the boundary of hemozoin crystals in situ. https://doi.org/10.1101/2022.05.13.491750

Nakatani, K., Ishikawa, H., Aono, S., Mizutani, Y., 2014. Identification of Essential Histidine Residues Involved in Heme Binding and Hemozoin Formation in Heme Detoxification Protein from Plasmodium falciparum. Sci Rep 4, 6137. https://doi.org/10.1038/srep06137

Nakatani, K., Ishikawa, H., Aono, S., Mizutani, Y., 2013. Heme-binding properties of heme detoxification protein from Plasmodium falciparum. Biochemical and Biophysical Research Communications 439, 477–480. https://doi.org/10.1016/j.bbrc.2013.08.100

Noland, G.S., Briones, N., Sullivan, D.J., 2003. The shape and size of hemozoin crystals distinguishes diverse Plasmodium species. Molecular and Biochemical Parasitology 130, 91–99. https://doi.org/10.1016/S0166-6851(03)00163-4

Olivier, M., Van Den Ham, K., Shio, M., Kassa, F., Fougeray, S., 2014. Malarial Pigment Hemozoin and the Innate Inflammatory Response. Frontiers in Immunology 5.

Pagola, S., Stephens, P.W., Bohle, D.S., Kosar, A.D., Madsen, S.K., 2000. The structure of malaria pigment β-haematin. Nature 404, 307–310. https://doi.org/10.1038/35005132

Schneider, S., Marles-Wright, J., Sharp, K.H., Paoli, M., 2007. Diversity and conservation of interactions for binding heme in b-type heme proteins. Nat. Prod. Rep. 24, 621–630. https://doi.org/10.1039/B604186H

Sheldrick, G.M., 2015. Crystal structure refinement with SHELXL. Acta Cryst C 71, 3–8. https://doi.org/10.1107/S2053229614024218

Solomonov, I., Osipova, M., Feldman, Y., Baehtz, C., Kjaer, K., Robinson, I.K., Webster, G.T., McNaughton, D., Wood, B.R., Weissbuch, I., Leiserowitz, L., 2007. Crystal Nucleation, Growth, and Morphology of the Synthetic Malaria Pigment β-Hematin and the Effect Thereon by Quinoline Additives: The Malaria Pigment as a Target of Various Antimalarial Drugs. J. Am. Chem. Soc. 129, 2615–2627. https://doi.org/10.1021/ja0674183

Straasø, T., Kapishnikov, S., Kato, K., Takata, M., Als-Nielsen, J., Leiserowitz, L., 2011. The Role of the Four Stereoisomers of the Heme Fe–O Cyclic Dimer in the Crystalline Phase Behavior of Synthetic Hemozoin: Relevance to Native Hemozoin Crystallization. Crystal Growth & Design 11, 3342–3350. https://doi.org/10.1021/cg200410b

Straasø, T., Marom, N., Solomonov, I., Barfod, L.K., Burghammer, M., Feidenhans'l, R., Als-Nielsen, J., Leiserowitz, L., 2014. The Malaria Pigment Hemozoin Comprises at Most Four Different Isomer Units in Two Crystalline Models: Chiral as Based on a

Biochemical Hypothesis or Centrosymmetric Made of Enantiomorphous Sectors. Crystal Growth & Design 14, 1543–1554. https://doi.org/10.1021/cg401151f
Tkatchenko, A., DiStasio, R.A., Car, R., Scheffler, M., 2012. Accurate and Efficient Method for Many-Body van der Waals Interactions. Phys. Rev. Lett. 108, 236402. https://doi.org/10.1103/PhysRevLett.108.236402
Weissbuch, I., Addadi, L., Berkovitch-Yellin, Z., Gati, E., Weinstein, S., Lahav, M., Leiserowitz, L., 1983. Centrosymmetric crystals for the direct assignment of the absolute configuration of chiral molecules. Application to the .alpha.-amino acids by their effect on glycine crystals. J. Am. Chem. Soc. 105, 6615–6621. https://doi.org/10.1021/ja00360a012
Wendt, C., de Souza, W., Pinheiro, A., Silva, L., de Sá Pinheiro, A.A., Gauvin, R., Miranda, K., 2021. High-Resolution Electron Microscopy Analysis of Malaria Hemozoin Crystals Reveals New Aspects of Crystal Growth and Elemental Composition. Crystal Growth & Design 21, 5521–5533. https://doi.org/10.1021/acs.cgd.1c00087
Winter, G., Waterman, D.G., Parkhurst, J.M., Brewster, A.S., Gildea, R.J., Gerstel, M., Fuentes-Montero, L., Vollmar, M., Michels-Clark, T., Young, I.D., Sauter, N.K., Evans, G., 2018. DIALS: implementation and evaluation of a new integration package. Acta Cryst D 74, 85–97. https://doi.org/10.1107/S2059798317017235
Wolf, S.G., Houben, L., Elbaum, M., 2014. Cryo-scanning transmission electron tomography of vitrified cells. Nat Meth 11, 423–428. https://doi.org/10.1038/nmeth.2842
World Health Organization, 2021. World malaria report [WWW Document]. URL https://www.who.int/publications-detail-redirect/9789240040496 (accessed 5.19.22).